Remote Sens. **2012**, *4*, 1-x manuscripts; doi:10.3390/rs40x000x

OPEN ACCESS

Remote Sensing

ISSN 2072-4292

www.mdpi.com/journal/remotesensing

Article

Mapping vegetation density in a heterogeneous river floodplain ecosystem using pointable CHRIS/PROBA data

Jochem Verrelst [1,*], Erika Romijn [2] and Lammert Kooistra [2]

[1] Image Processing Laboratory, Department of Earth Physics and Thermodynamics, University of Valencia, P.O. Box 22085, E-46071 Paterna (Valencia), Spain; Email: jochem.verrelst@uv.es (J.V.)

[2] Laboratory for Geo-Information and Remote Sensing, Wageningen University and Research Centre, Droevendaalsesteeg 3, 6708 PB Wageningen, Netherlands. Emails: erika.romijn@wur.nl (E.R.); lammert.kooistra@wur.nl (L.K.)

***** Author to whom correspondence should be addressed; E-Mail: jochem.verrelst@uv.es (J.V.); Tel.: +34-96-354-4067; Fax: +34-96-354-3261.

Received: / Accepted: / Published:

Abstract: River floodplains in the Netherlands serve as water storage area, while they also have the function of nature rehabilitation area. Floodplain vegetation is therefore subject to natural processes of vegetation succession, which obstructs the water flow into the floodplains and increases the flood risk for the hinterland. Space-based pointable imaging spectroscopy has the potential to quantify vegetation density from a desired view zenith angle. In this respect, hyperspectral pointable CHRIS data were linked to the ray tracing canopy reflectance model FLIGHT to retrieve vegetation density estimates over a heterogeneous river floodplain. FLIGHT enables to simulate top-of-canopy reflectance of vegetated surfaces either in turbid (e.g. grasslands) or in 3D (e.g. forests) mode. By inverting FLIGHT against CHRIS data, the vegetation density parameter leaf area index (LAI) was computed for three main classified vegetation types, ‘herbaceous’, ‘shrubs’ and ‘forest’, and for the CHRIS view zenith angles in nadir, backward (-36°) and forward (+36°) scatter direction. The -36° direction showed most LAI variability within the vegetation types and was best validated, closely followed by the nadir direction. The +36° direction led to poorest LAI retrievals. The class-based inversion process has been implemented into a GUI toolbox which would enable the river manager to generate LAI maps in a semiautomatic way.

Keywords: pointable sensors; CHRIS/PROBA; leaf area index (LAI); inversion; radiative transfer (RT) model; FLIGHT; river floodplain ecosystem; vegetation density

1. Introduction

Climate change is expected to have a large impact on water resources and flooding risks of the main rivers in the Netherlands [1]. General circulation models applied on the Rhine river basin predict higher winter discharge and peak flows as a result of increased winter precipitation and earlier snow-melt in the Alps [2,3]. In the past, measures for improvement of river navigation, as well as agricultural development have caused the Rhine to lose its natural meanders while significant parts of the floodplain have been affected by urban development [4,5]. As a result, the capability of the river system to accommodate peak flows has been reduced which leads to increased flooding risks for the floodplains and its hinterland [6].

During the last decades, the water discharge capacity of the river system in the Netherlands has been increased by lowering and widening of the floodplains, removal of groynes and hydraulic obstacles in the floodplains and by excavation of secondary channels [7,8]. Concomitantly, these newly developed river floodplains also serve as nature restoration areas, where succession of vegetation leads to highly valued ecosystems [9]. However, floodplain vegetation causes resistance to the water flow within the river floodplains [10]. Because of the complex structure of floodplain vegetation and the accumulation of material caused by sedimentation processes, flood flow velocities decrease and the water surface increases during flooding events [11]. For assessment of current and future river management scenarios in low land rivers like the Rhine in the Netherlands, information on the spatially complex structure and density of floodplain vegetation is a key issue [12].

To intervene with the spontaneous vegetation succession, the concept of Cyclic Floodplain Rejuvenation (CFR) has been introduced for management of the Rhine river system [13]. CFR implies periodic anthropogenic disturbance of floodplain ecosystems through removal of climax vegetation to create more space for water. To support this approach, regular monitoring of the spatial distribution and structure of floodplain vegetation is required for estimating the hydraulic roughness within the floodplain. Hydraulic roughness indicates to what extent the water flow is obstructed and is directly related to vegetation height and density, rigidity of the stems and the presence of leaves [12,13]. For the rivers Rhine and Meuse in the Netherlands, ecotope maps are used for determining hydraulic roughness values of the vegetation, resulting in one roughness value per ecotope object. Currently, ecotope maps are based on digital false colour aerial photographs and ancillary *in situ* data on flood

duration, management, water depth and morphodynamics [14]. However these techniques are tedious and time-consuming and no information on spatial variability of vegetation density within the ecotopes is provided.

Alternatively, satellite based Earth observation (EO) can play a major role by providing a quantifiable, spatially-explicit and replicable technique for monitoring and assessing the magnitude of vegetation density. With optical EO data, vegetation properties can be characterised into a few essential structural variables such as leaf area index (LAI), defined as the total of one-sided area of leaves per area (m^2/m^2) [15]. Within this approach for approximating hydraulic roughness, LAI provides continuous vegetation density information at the pixel level. Implementing LAI in hydraulic roughness calculation schemes may bypass the need for many elaborative field measurements [16].

The retrieval of LAI from EO data is often based on empirical relationships between spectral vegetation indices and ground-based measurements [17,18]. These relationships work well under particular viewing and illumination geometry and for specific vegetation phenology, but they tend to produce inaccurate results when applied over a broad range of land cover types and optical and geometric conditions encountered in satellite images. Canopy reflectance is the result of several intricately coupled physical processes and it is therefore difficult to estimate the influence of a single parameter from experimental data (e.g., [19]). Contrary to empirical approaches, radiative transfer (RT) models take the physical features of a plant canopy into account and are therefore more realistic in describing the interaction of solar radiation with vegetation components. From a radiative transfer point of view, a vegetation canopy composed of components like leaves, stems, flowers, etc., can be considered as an ensemble of scattering elements, bounded by a background, e.g., soil [20]. A physical RT model describes the transfer and interactions of solar radiation inside such a canopy and thus provides an explicit link between the structural characteristics of vegetation scattering elements and the canopy reflectance. In these RT models the spectral signal is a function of canopy geometry, defined by canopy structural variables such as LAI, leaf angle distribution and fractional vegetation cover, optical leaf and soil properties, illumination and viewing geometry [21-23]. LAI is a typical state variable of RT models, describing the density of the scattering elements. In turn, these biophysical variables can be extracted from RT models through model inversion.

Among RT models, FLIGHT [24] is a physical three dimensional (3D) ray tracing model based on Monte Carlo simulations of photon transport. FLIGHT is accurate in mimicking vegetation structure: it simulates interactions between geometric primitives representing the canopy and solar radiation on a photon-by-photon basis. Inversion of the model against measured reflectance data allows retrievals of LAI at the sensor sub-pixel scale.

Apart from the expected enhancement of the physical RT modelling approach for retrieval accuracy, additional gains are to be expected with the use of pointable sensors. Canopy reflectance measurements acquired under different observation angles have shown to yield unique information pertaining to vegetation structure [25-31]. The presence of shadows in the canopy forms an important argument for exploring pointable data because the shadowing effect in vegetated surfaces will result in enhanced reflectance in the backscatter direction and reduced reflectance in the forward scatter direction of the principal plane [32]. Hence, observed variation in reflectance anisotropy is a function of sun-target-sensor geometry and the composition and structure of the vegetation cover. Therefore, the combined use of RT methods with pointable imaging spectroscopy data may lead to a more robust approach to map the complex floodplain vegetation structure and density from space.

The ESA's Compact High Resolution Imaging Spectrometer (CHRIS) on board the Project for On Board Autonomy (PROBA) satellite is a pointable, imaging spectroscopy sensor that was designed as a technology demonstrator [28]. CHRIS is capable of measuring reflected radiation in the visible and near-infrared (NIR) wavelengths from five different viewing angles by pointing five times to the same target during a single overpass. The sensor can be configured in different imaging modes with specific spectral and spatial settings. Especially, mode 3 is appropriate for vegetation structure mapping as it is characterized by both a high spatial (~17m) and high spectral resolution with 18 bands measuring in the visible and NIR wavelengths from 400 to 1050 nm, thereby covering a region of 13 by 13 km (full swath) [28].

Several studies have been performed using pointable CHRIS data combined with an RT modelling approach to derive LAI values for homogeneous vegetation stands in agricultural fields [33-34]. FLIGHT has proven to be successful in combination with angular CHRIS data and its use for retrieving vegetation structure because of simulating vegetated surfaces at the same spatial resolution [19,35]. However, research on quantitative vegetation density retrieval in heterogeneous floodplain ecosystems, taking into account different vegetation types such as species-rich grasslands grading towards shrub and tree encroachments, have rarely garnered attention in the scientific literature.

In this study we aim at characterizing the vegetation density of a spatially and spectrally complex river floodplain ecosystem using angular CHRIS data. The objective is threefold: *i*) to develop a methodology for physically-based mapping of the density variable LAI of several vegetation types in a river floodplain ecosystem using FLIGHT; *ii*) to explore the added value of the use of the pointable dimension in the applied methodology; and *iii*) to assess the opportunities to upscale the methodology developed for a local floodplain to a complete river section at the regional scale.

2. Materials and Methods

2.1. Study site

The study site is the floodplain Millingerwaard (51° 84' N, 5° 99' E) along the river Waal, which is the main branch of the river Rhine in the Netherlands (figure 1). Millingerwaard (700 ha) is one of the main floodplains of the nature reserve Gelderse Poort, with a total surface area of 6700 hectare. Within the Netherlands, the Gelderse Poort serves as important riparian corridor within the Natura 2000 network of the European Union. Before 1990, Millingerwaard was used as an agricultural area with intensively managed grassland and arable crops (e.g., maize). Starting from 1990, agricultural management was gradually reduced and a nature rehabilitation plan was started. By digging out clay deposits from the topsoil, the old patterns of side streams, natural levees and isles were reconstructed in the landscape. Floodplain vegetation was going through natural succession and a regime of grazing by cattle and horses in low densities was introduced. Current vegetation of the Millingerwaard floodplain consists of mixed patches and ecotones, i.e. transitions between communities with a dominance of grass, herbaceous vegetation, dwarf and tall shrubs, and a large softwood forest [36]. Softwood forest in Millingerwaard is dominated by willow trees (*Salix fragilis* and *Salix alba*). The forest canopy has an open structure with dense undergrowth (*Urtica dioica* (stinging nettle), *Arctium lappa* (greater burdock), *Galium aparine* (cleavers)) and open water bodies due to the low elevation and high ground water levels. The non-forest vegetation is characterized by a heterogeneous patchy structure of different vegetation succession stages. Dominant species are *Urtica dioica, Calamagrostis epigejos* (wood small-reed), *and Rubus caesius* (dewberries). Finally, a limited number of parcels is still in agricultural use. Vegetation types present in Millingerwaard are representative for the vegetation succession stages of the other floodplains within the Gelderse Poort nature reserve. At this moment, the surface area of agricultural land in the complete Gelderse Poort is relatively high compared to that of the Millingerwaard, however, this will change over the coming decade as agricultural management will be changed to a nature management regime.

Figure 1. The study area which is located in the east of the Netherlands, indicated on the CHRIS nadir image in true colour band composition (R: 675.2 nm, G: 551.7 nm, B: 490.5 nm). The red circle represents the river floodplains of Millingerwaard. The black outlined river area overlain on the CHRIS nadir image represents the nature reserve the Gelderse Poort which was used for upscaling of the method.

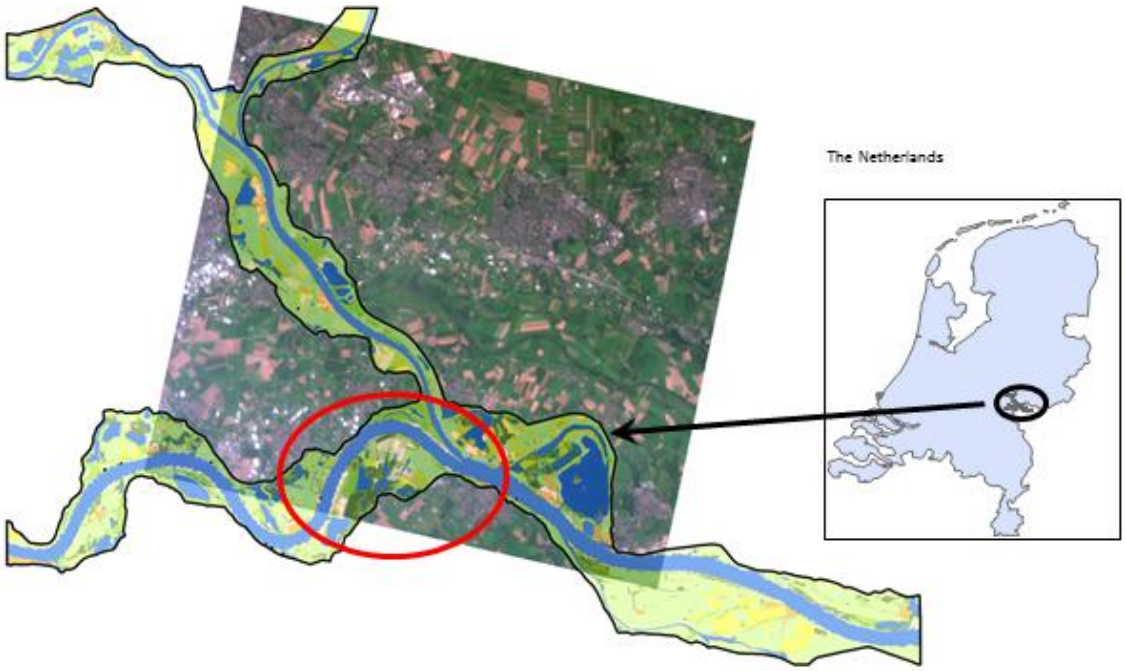

2.2. CHRIS data

Concomitant pointable CHRIS images for the Millingerwaard and a large part of the Gelderse Poort (figure 1) were acquired on 6 September 2005 in mode 3 under cloud-free conditions around solar noon. Data were available in five different nominal viewing zenith angles (VZA): nadir, ±36º, ±55º. The pointable observations are named as such hereafter. The actual position of the sensor during the satellite overpass is shown in the polar plot of figure 2. Negative viewing angles represent measurements in the backscatter direction, where most sunlit canopy is viewed by the sensor; positive viewing angles represent measurements in the forward scatter direction, where most shadowing effects are present. The solar zenith angle during acquisition was 46º. For the purpose of this research, the images of VZA nadir and ±36º were used, because the ±55º angular images did not cover the Millingerwaard study area.

Figure 2. Polar plot showing the actual positions of the 5 angular CHRIS images during acquisition on 6 September 2005. The solar zenith angle was 46°, the solar azimuth angle 170°.

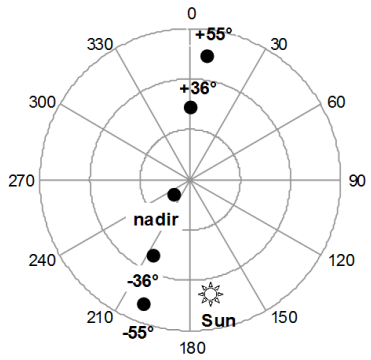

Automatic image registration of the CHRIS nadir and ±36º images was performed according to the method of [37] to reference the three separate images to each other. Geometric correction of these three images was carried out with use of 34 ground control points (GCP's) which were collected from a high spatial resolution (0.5 m) aerial photograph from early spring 2006. Because the CHRIS images were already referenced to each other, the GCP's were taken from the nadir image only and also applied to the ±36º images. A 2nd order polynomial model with nearest neighbourhood resampling technique was used for geometric correction of the three images which resulted in a control point error of 0.31 pixels. Atmospheric correction of the images was performed according to the method described by [38] using the CHRIS-Box software developed as a plug-in for the BEAM toolbox (Brockmann Consult, http://www.brockmann-consult.de/beam).

2.3. Land cover classification of CHRIS nadir image

Prior to vegetation density retrieval in canopies comprised of a heterogeneous mix of vegetation types, these vegetation types need to be identified so that the RT model can be parameterized accordingly. Such vegetation class-based inversion approach is operationally being done at a global scale to derive MODIS products [39] and was recently introduced by [40] at local scale for precision farming applications. Here, using information from the three observation angles, a map was created that included eight major land cover classes. The vegetated classes consisted of 'bare and pioneer communities', 'grasses and herbaceous vegetation', 'herbaceous and low woody vegetation', 'shrubs', and 'forest'. These classes are in accordance to the class definitions used by [41] that serve as a minimum set to estimate hydraulic resistance for river management purposes. The class 'forest' represents the areas that consist of pixels with tree cover. The classes 'water', 'build up area', and 'arable land' were added to be able to classify the whole CHRIS image. A summary of all classes and their main characteristics is listed in table 1, the undertaken steps are shortly explained below.

Table 1. Classes used for classification of the CHRIS image.

	Class name	Class characteristics
1	Bare soil & pioneer vegetation	mainly sand
2	Grasses and low herbaceous vegetation	vegetation < 1m
3	Higher herbaceous vegetation	vegetation between 1m and 2m
4	Shrubs	shrubs and trees < 5m
5	Forest	trees > 5m
6	Water	water
7	Build up	streets, houses
8	Arable land	maize

Maximum likelihood (ML) classification was performed on the CHRIS nadir image to classify the identified land cover classes within the boundaries of Millingerwaard (figure 1). First, a training data set was defined on which the classification was based. Regions of interest (ROIs) were selected as training data for each land cover class. The CHRIS nadir image was used to roughly discriminate between classes. Field knowledge and aerial photographs of early spring 2006 were used as reference for selecting ROIs. The principal component (PC)-bands of the stacked images (nadir and VZA ±36º) were very useful to identify sharp boundaries between different land cover classes; because certain PC-band combinations showed bright colourful images which made it easy to distinguish the different land cover types. The selection of ROIs was evaluated by computing ROI separability based on the transformed divergence and Jeffries-Matusita Distance of the whole visible and NIR (VNIR) spectrum from the CHRIS nadir image. The separability values showed that the pair of 'higher herbaceous vegetation' and 'grasses and low herbaceous vegetation' had highly comparable spectral characteristics.

The aerial photographs of 2006 were used as basis for selection of data-points to validate the classification result of the major land cover classes. A set of twenty random sample points was selected per class resulting in the selection of 160 points in total. The distance between two points was set to a minimum of 100 m to prevent choosing points located too close to each other. A difficulty with the use of aerial photographs was to differentiate between 'low grasses & herbaceous vegetation' and 'higher herbaceous vegetation'. Based on field knowledge, and the assumption that patches of grasslands with an irregular shape consisted of taller grasses and herbaceous vegetation, those patches were labelled to the class of 'higher herbaceous vegetation'. Finally, classification accuracies and the kappa statistic were calculated for the classified land cover map.

243 *2.4 FLIGHT model inversion to derive LAI*

244

245 The ray tracing FLIGHT model simulates photon trajectories, starting from a solar source, through
246 successive interactions with the vegetation, to a predetermined sensor viewing angle [24]. The model
247 incorporates the probability of free path, absorption and scattering of photons and accounts for
248 shadowing effect, crown overlapping and multiple scattering between crowns. Within the crown,
249 photons are scattered based on probability density functions. The individual photons are followed until
250 they are either absorbed or exited by the canopy. The model outcome is scene top-of-canopy bi-
251 directional reflectance (BRF) values, the result of a unique stand configuration, solar illumination
252 direction, surface reflection direction and spectral wavelength (λ). FLIGHT can be operated either in
253 1D or 3D mode. In 1D mode, the vegetation canopy is modelled as turbid medium, which can be seen
254 as a layer that contains a mix of different canopy elements which represent the vegetation density
255 characteristics. Vegetation density of a scene is exclusively controlled by LAI. In 3D mode, the
256 vegetation canopy is modelled as a 3D representation of tree crowns, which are idealized by
257 volumetric primitives of defined shapes with associated shadowing effects. Vegetation density within
258 the volumetric primitives is controlled by LAI and the density of the primitives within a scene is
259 controlled by fractional vegetation cover. This 1D/3D flexibility enables to employ a better
260 representation of patchy landscapes, i.e., homogeneous areas can be simulated in 1D mode while
261 heterogeneous areas (e.g., 'forest') can be simulated in 3D mode.

262 The vegetation classes used in the classification were simplified to form a base map for the class-
263 based model inversion. From the five vegetation classes 'bare and pioneer communities'; 'grasses and
264 herbaceous vegetation'; 'herbaceous and low woody vegetation'; 'shrubs'; and 'forest', the vegetation
265 class 'bare soil and pioneer communities' was omitted from further analysis because this class does not
266 have a complex structure thus the influence on the hydraulic resistance can be neglected. The two
267 classes 'low grasses and herbaceous vegetation' and 'higher herbaceous vegetation' which showed a
268 relatively low separability were aggregated into one class of 'herbaceous' vegetation. This led to three
269 distinct vegetation classes 'herbaceous', 'shrubs' and 'forest', for parameterization of FLIGHT. The
270 'herbaceous' and 'shrubs' classes were parameterized in 1D mode because of its continuous horizontal
271 distribution, while 'forest' was parameterized in 3D mode. For each vegetation class, model
272 parameters; leaf, woody and background spectra; and LAI variable ranges were defined and fed into
273 FLIGHT (table 2). Vegetation model parameters were defined based on field measurements and ranges
274 of variables were defined based on findings in literature [42-44]. Leaf reflectance and transmittance
275 spectra were measured with an ASD field spectrometer during a field campaign in 2004. Also tree
276 geometry indicators were measured and are listed in table 2. We assumed that changes in leaf structure

and composition of willow trees (> 20 years old), as present in Millingerwaard, are small within a period of one year, and that therefore the field measurements match the reflectance spectra of leaves of willow trees in 2005. Additional reflectance spectra of various bark and background types were collected in April 2009 with an ASD field spectrometer. The spectra were resampled to the band settings of the CHRIS sensor.

Table 2. FLIGHT model parameters and variables, and input spectra.

Class name	Input spectra		
	Leaf	**Background**	**Bark**
Herbaceous	Calamagrostis epigejos	0.95*forest background + 0.05*sandy soil	
Shrubs	Salix alba	average (water, grass & forest background)	Salix alba
Forest	Salix alba	forest background	Salix alba

Class name	Variables		Fixed parameters		
	Fcover	**LAI (m^2/m^2)**	**PV**	**Scene**	**Leaf size (m)**
Herbaceous	0.2-1; step: 0.02	0.2-10; step: 0.1 until 5; step: 0.5 until 10	1	1D	0.027
Shrubs	0.2-1; step: 0.02	0.2-10; step: 0.1 until 5; step: 0.5 until 10	0.7	1D	0.02
Forest	0.2-1; step: 0.02	0.2-10; step: 0.1 until 5; step: 0.5 until 10	0.7	3D	0.02

Fixed parameters tree geometry	
Crown shape	ellipsoid
crown radius	3
Centre to top distance	3
Height to first branch:	
Min:	1
Max:	4
Trunk DBH	0.4

Model inversion is required in order to retrieve vegetation characteristics from reflectance data through physically based models [45]. Inversion was accomplished by means of a lookup-table (LUT) approach [46]. The LUT provides a simple way of the inversion of a radiative transfer model and also reduces the computational demand compared to the traditional optimization approach [48,49]. For each VZA and each vegetation class a LUT containing simulated reflectance data was built by means of combining the canopy variables following the steps as provided in table 2. Given the LUT input parameters, FLIGHT subsequently computed the BRF for 18 spectral bands corresponding to the band settings of the CHRIS sensor. The inversion itself was done by first calculating the root mean square errors (RMSE) between each measured reflectance spectrum from the CHRIS nadir and ±36° images and all simulated BRF spectra as stored in the LUT. Because multiple variable combinations may lead to the same spectra (the problem of ill-posedness), the solution applied here is the average of variable

299 combinations found within less than 10% of the lowest RMSE value. The 10% threshold agrees with
300 several studies that attempted to optimize inversion (e.g., [49-51]). As such, LAI values were pixelwise
301 retrieved per vegetation class for the nadir and the ±36° VZAs. Additionally, RMSE residuals were
302 provided to obtain information about the performance of the retrievals. The residuals reveal the
303 closeness of actual spectral observations to that of the simulated spectra in the inversion; lower
304 residual means a better match. This enabled to compare differences in retrieval performances between
305 angles. Finally, for each of the three viewing angles the maps with the class-specific retrievals from the
306 herbaceous, shrubs and forest class were aggregated in order to generate LAI maps for the entire area
307 of Millingerwaard.

308 An essential step in asserting the appropriateness of optical EO measurements to partake in the
309 characterization of vegetation density variables is to seek evidence in the validity of the variables.
310 Validation of LAI measurements were derived from a ground sampling campaign which was carried
311 out in first two weeks of august 2004 in the Millingerwaard [52]. The dataset consisted of 13 sample
312 plots of 20x20 m in the forest area, which were selected following a random sampling scheme with a
313 minimum of 20 m distance from each other. Each plot was set up according to the VALERI
314 (Validation of Land European Remote Sensing Instruments) protocol [53] and consisted of 12
315 measurement points per plot. At each point within the plot one measurement in 180° upward direction
316 and one measurement in 180° downward direction were taken with the hemispherical camera. The
317 hemispherical photographs were processed with use of the neural network based software CAN_EYE
318 to calculate the gap fraction and to derive the clumping factor and true LAI values [54]. The validation
319 dataset from 2005 consisted of 16 sample plots of 20x20 m with more or less homogeneous vegetation
320 cover in herbaceous, shrubs and forest vegetation. The sample plots were also set up according to the
321 VALERI protocol. The effective LAI was estimated with use of hemispherical photography and
322 subsequently corrected into true LAI values with use of the average clumping index per plant-
323 functional type from TRAC (Tracing Radiation and Architecture of Canopies) measurements and
324 woody-to-total area ratio from the hemispherical photographs [55].
325
326 *2.5 Upscaling of the method*
327
328 Finally, the methodology was upscaled to all floodplains within the complete river section of the
329 Gelderse Poort nature reserve (figure 1). RT models are not limited to site or sensor-specific
330 dependencies [56] and can therefore be applied to larger floodplain areas without having to
331 compromise on the retrieval quality. First, a land cover classification was made, based on the same
332 training dataset which was used for the Millingerwaard. Thereafter, FLIGHT model inversion was

333 applied per vegetation class for the Gelderse Poort to derive LAI values. Because of the class-based
334 inversion approach and the broad range of simulations present in the LUT for each vegetation class,
335 covering a large variety of plausible canopies, no additional adjustments had to be made to upscale the
336 same methodology to the larger floodplain area. Finally, in view of applying the class-based model
337 inversion approach to images from any imaging spectrometer, the whole methodology has been
338 implemented into a Matlab-based graphical user interface (GUI) toolbox called ARTMO (Automated
339 Radiative Transfer Models Operator) [57]. Hence, with ARTMO LAI maps can be obtained in a
340 semiautomatic way thereby taking the distinct nature of different land cover classes into account.
341
342 **3. Results**
343 *3.1 Classification*
344
345 The classified land cover map of the CHRIS nadir image for the Millingerwaard is presented in
346 figure 3b and has an overall accuracy of 68% and a kappa coefficient of 0.56 (table 3). Notably, most
347 misclassifications occurred between the ‘grasses and herbaceous vegetation’ and the ‘herbaceous and
348 low woody vegetation’, because the spectral characteristics of these classes have similarities and
349 mixing of different vegetation types occurred in the pixels (~17 m) of the CHRIS image. When
350 merging these two classes, the overall accuracy improved to 73%. The largest part of Millingerwaard
351 was covered by grasses and (low and higher) herbaceous vegetation. Some parts of the river
352 floodplains have recently been excavated and consisted of bare soil. Shrubs and softwood forest
353 surrounded the lakes. Some pieces of land in the eastern part with a rectangular shape and
354 homogeneous land cover represented arable land and agricultural grassland. The remaining part of the
355 area had a heterogeneous land cover with transitions between land cover types on the pixel-level which
356 is characteristic for a natural river floodplain ecosystem.
357
358

Figure 3. Maximum likelihood classification result of the CHRIS nadir image of the (**a**) Gelderse Poort and (**b**) Millingerwaard (indicated with the black square) into major land cover types.

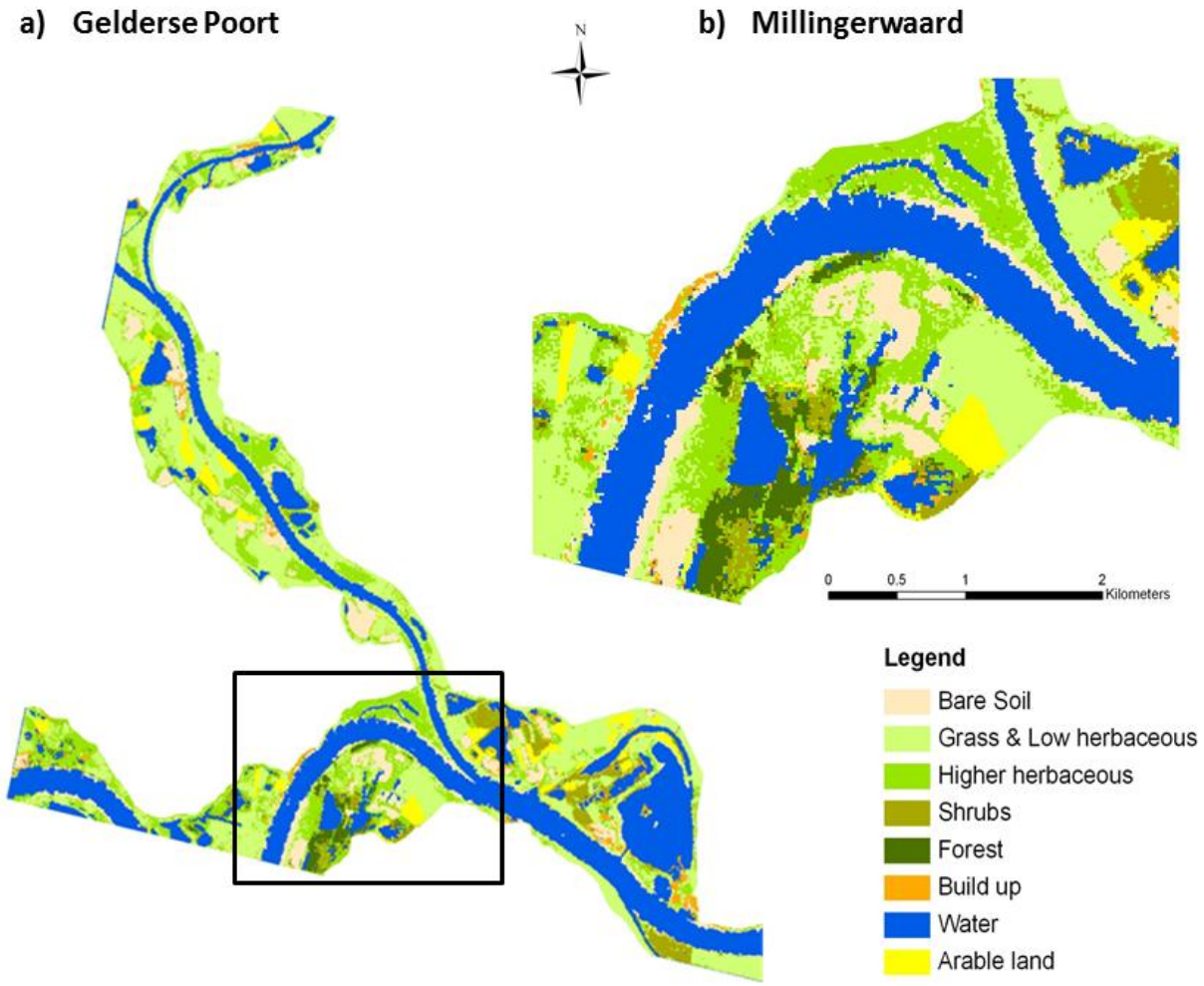

Table 3. Accuracy matrix of CHRIS nadir maximum likelihood classification.

Classified data	**Reference data**								
	Bare soil	**Grass & low herbaceous**	**Higher herbaceous**	**Shrubs**	**Forest**	**Agricultural**	**Water**	**Build up**	**User's accuracy**
Bare soil	11	3	0	0	0	1	3	2	55%
Grass & low herbaceous	0	19	1	0	0	0	0	0	95%
Higher herbaceous	1	6	8	2	2	0	1	0	40%
Shrubs	0	5	1	9	4	0	1	0	45%
Forest	2	1	0	1	16	0	0	0	80%
Agricultural	0	3	0	0	0	17	0	0	85%
Water	0	1	0	0	1	0	18	0	90%
Build up	3	1	1	0	3	1	0	11	55%
Producer's accuracy	65%	49%	73%	75%	62%	89%	78%	85%	

368 *3.2 Vegetation class based angular LAI retrievals*
369
370 LAI maps were generated through model inversion for the vegetation cover classes of 'herbaceous',
371 'shrub' and 'forest' vegetation within the Millingerwaard study site. LAI results for herbaceous, shrub
372 and forest vegetation were combined into a single map for each viewing direction (figure 4 [left]).
373 White parts in the maps represent areas that were not included in one of the three vegetation classes.
374 Large variation in retrieved LAI values could be observed within all the three classes in the river
375 floodplain area, which reinforces the significance of quantifying density at the pixel level. Largest LAI
376 variability was obtained in the -36º VZA, closely followed by the nadir direction, whereas the variation
377 of the inverted values was considerably lower for +36º VZA. Spurious high LAI values between 8 and
378 9 occurred in several fields and along the dikes. Due to their rectangular shape and homogeneous land
379 cover (figure 3) it could be deduced that these dense vegetated areas are probably related to intensively
380 managed agricultural grasslands. Similar orders of magnitude were observed along the dike in the
381 south of Millingerwaard, also due to agricultural use (grassland or maize). These agricultural areas are
382 excluded in further analysis. The generated histograms show the LAI distribution of the river
383 floodplain for the three viewing angles (figure 4[right]). From these histograms it can be observed that
384 nadir failed to identify pixels with very low LAI (<1), which are present over the sandy river banks. In
385 case of -36 VZA, LAI values ranged between 0.3 and 6 for the shrubs and herbaceous areas. Large
386 variations were obtained within the herbaceous vegetation class west of the lakes. Peaks in LAI
387 indicated the spatial pattern of shrub encroachment, where the highest values belonged to the fast
388 growing shrub *Crataegus monogyna* (hawthorn). Also the shrub class around the lakes showed great
389 variation in LAI. This concerned mainly *Salix* (willow) species which vary in density and height. The
390 forest class, which was simulated in 3D, yielded LAI values within a narrow range, between 5 and 7.
391 When validating the LAI results, it can be observed from the scatter plots (figure 5) that the nadir
392 and -36º VZA performed alike, with a somewhat better RMSE accuracy for -36º VZA. The RMSE
393 accuracies were 1.05 for -36º VZA and 1.23 for nadir respectively. For both viewing angles the
394 retrieved LAI values were overall closely positioned to the 1:1-line. The retrieved LAI values fell
395 within the same range between 2 and 7 as the LAI values obtained with the hemispherical camera
396 (figure 5). Though, it has to be noted that over the pixels labelled as forest hardly variation in LAI was
397 detected. Conversely, the +36º VZA led to considerably poorer accuracies (RMSE: 2.63), suggesting
398 that this viewing angle leads to suboptimal retrievals.
399 Another way of evaluating the performances of the LAI retrievals is inspecting the RMSE residuals,
400 which were mapped in figure 6 [left]. Although no validation *per se*, these RMSE maps can give us a
401 better spatial understanding of the success of the inversion process. When comparing the viewing

angles it can be noted that nadir and -36º VZAs performed alike, while forward scatter +36º VZA had more difficulty with the inversion. The latter not only led to overall poorer residuals but also delivered considerably more patches with very poor retrievals (dark red spots). This implies that some degree of mismatch between actual spectra and the simulated spectra took place. It suggests that either FLIGHT was not well able to represent the complex shadowing effects in this direction or that a more accurate atmospheric correction regime is needed at this angle. The RMSE maps also suggested that there were no indications that one vegetation class performed worse than the other classes; the image was consistently inverted with some patches (dark red spots) of poorer residuals. These patches typically emerged on landscape edges or on areas with high LAI retrievals. Finally, when looking closer to the residuals at nadir and -36º, despite some patches of poor retrievals, -36º VZA showed slightly better performances throughout the whole image. This can also be observed in the histograms of the residual maps (figure 6 [right]), where the -36º VZA led to considerably more pixels with very low RMSE values (very left part of histogram).

Figure 4. LAI maps (left) and derived histograms for LAI<8.5 (right) of Millingerwaard for the backward scattering direction (-36° VZA) (top), the nadir direction (middle) and the forward scattering direction (+36° VZA) (down), derived with FLIGHT model inversion.

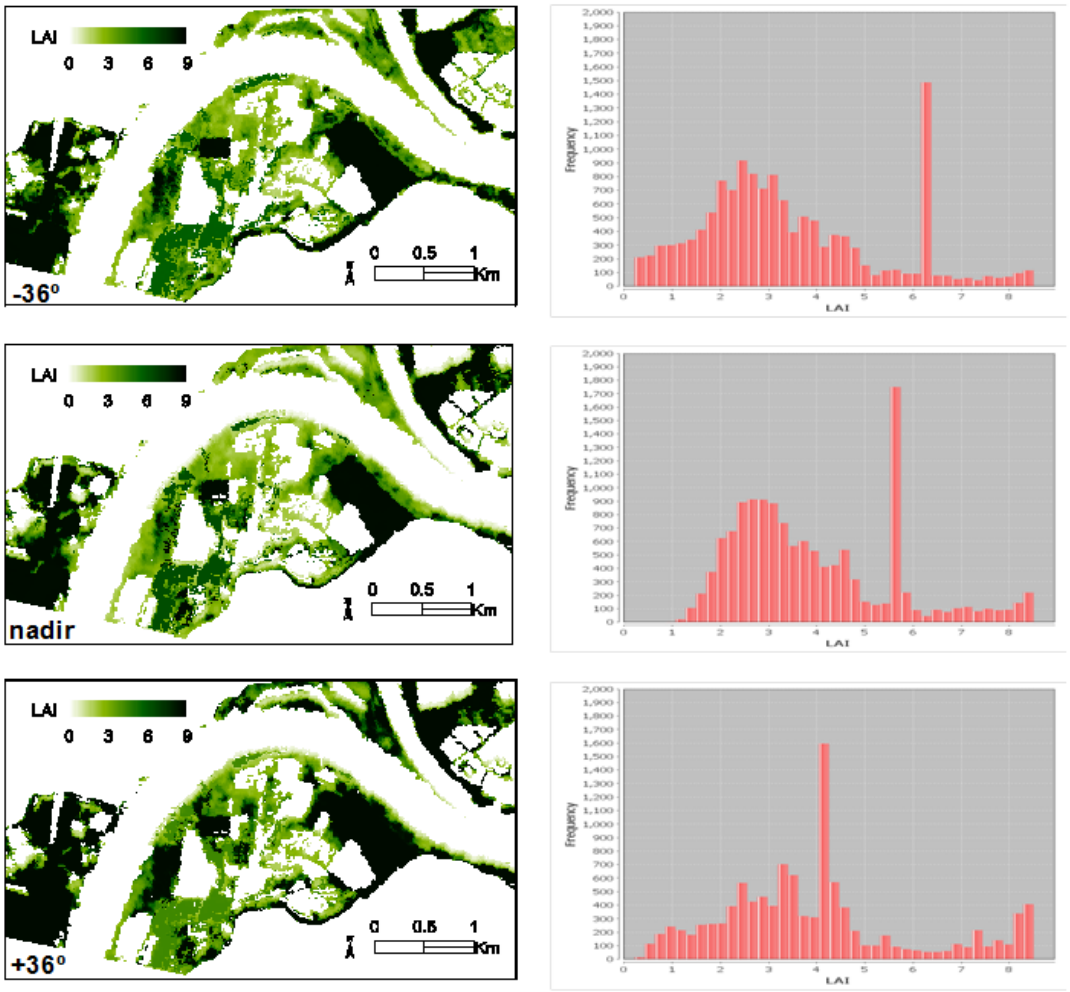

Figure 5. Validation results of the estimated LAI obtained with FLIGHT model inversion, plotted against the measured LAI values obtained with the hemispherical camera for the backward scattering direction (-36° VZA), the nadir direction and the forward scattering direction (+36° VZA).

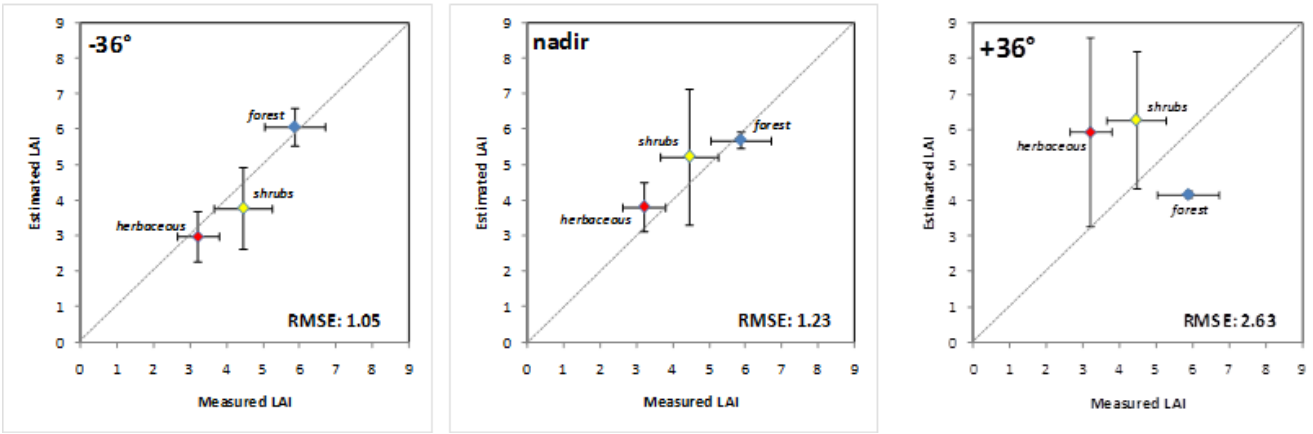

Figure 6. Maps of minimum RMSEs for LAI retrievals (left) and derived histograms for <8.5 (right) of Millingerwaard for the backward scattering direction (-36° VZA) (top), the nadir direction (middle) and the forward scattering direction (+36° VZA) (down), derived with FLIGHT model inversion.

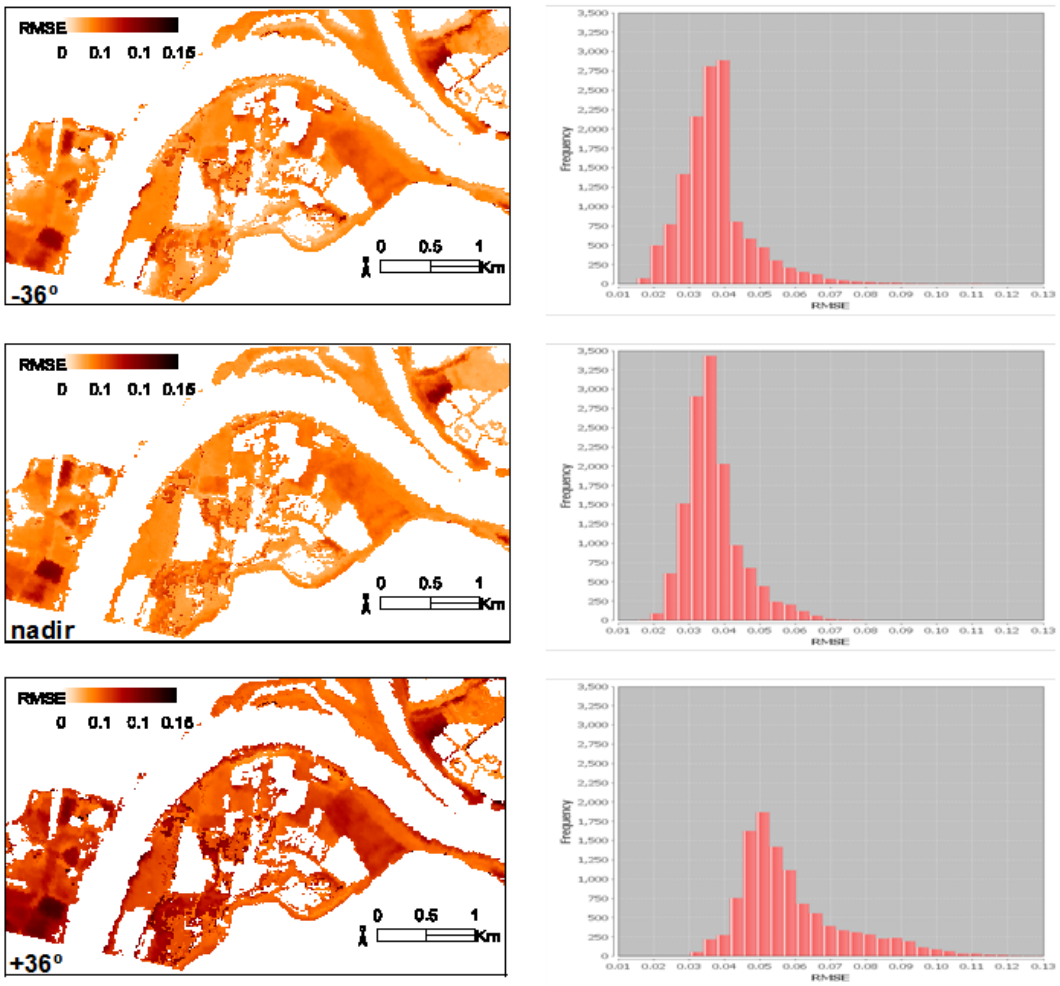

3.2 Upscaling LAI maps to the larger floodplain 'Gelderse Poort'

To demonstrate the portability of the class-based model inversion, the complete methodology was applied to the larger floodplain area of the Gelderse Poort nature reserve. This resulted first in a land cover map (figure 3a) and subsequently LAI maps for the three viewing angles for this area. The land cover map reveals that most natural vegetation is present in the southern part of the land cover map. The Millingerwaard floodplain is located here, but the landscape is also characterized by patches of semi-natural grasslands, shrubs, bare soil and lakes and agricultural fields. To the North, the landscape is dominated by agricultural crops and grasslands. These parts have not yet been subject to the natural management regime. The map formed the basis for the class-based LAI retrieval. Figure 7 shows as an example of the LAI map for the -36º VZA, the viewing angle that was best validated and where most variability was perceived. Generated LAI values over the larger floodplain were within the same range as over the Millingerwaard. Large LAI variability can be observed in the more natural areas, especially in the South and South-eastern part of the map, but also in some parts along the river in the centre and North of the map. More northwards, where more agricultural fields were present, areas of high LAI values suggest that these parcels consisted of homogeneous agricultural vegetation cover, such as mature maize fields.

Figure 7. LAI map and histogram for the backward scattering direction (-36˚ VZA), derived with FLIGHT model inversion after upscaling to the Gelderse Poort area.

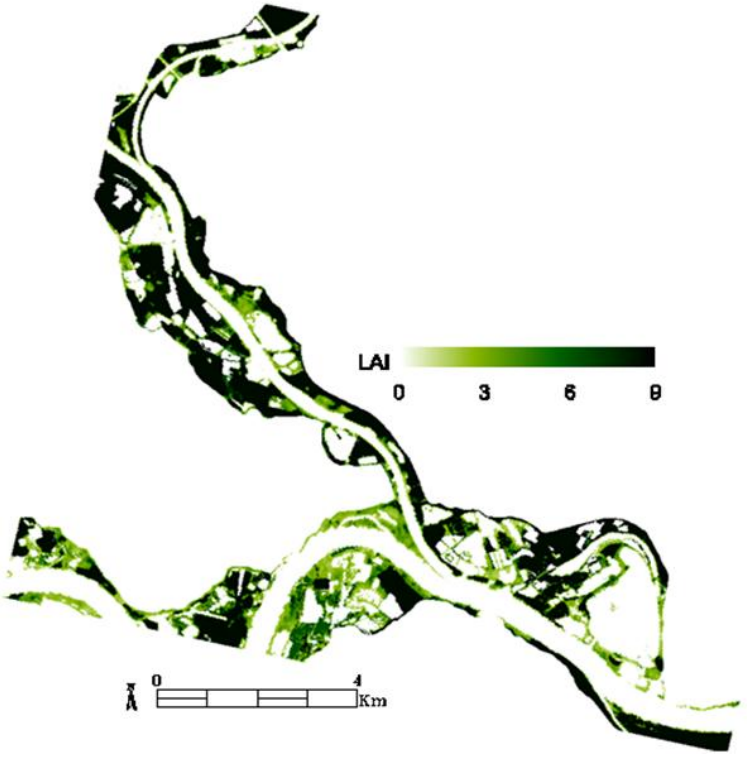

4. Discussion

New methods are required to automate approaches and streamline the tedious process of hydraulic roughness calculation for vegetation in river floodplains [14]. The overall goal of this study was to develop and test a methodology for spatially-explicit estimation of vegetation density using data from pointable EO spaceborne platforms. In the next sections, first the characterization of vegetation density in terms of LAI for a river floodplain, and next the proposed approach of customized model inversion against pointable, imaging spectroscopy data will be discussed in more detail. Finally, the discussion will be closed with recommendations towards operational river floodplain monitoring.

4.1. Vegetation density characterization

LAI is one of the main biophysical variables that can be derived from space [15]. At the same time, LAI can be considered as an important proxy of vegetation density, e.g. for the calculation of hydraulic roughness of river floodplains. Specifically the vegetated areas with high LAI have potential to generate a high accumulation of biomass, and are most critical for the estimation of the hydraulic conductivity of the floodplain. For these areas removal of vegetation under the Cyclic Floodplain Regime could be considered [13]. Moreover, deriving LAI from pointable observations may be beneficial compared to conventional nadir observation because of the ability of controlling the contribution of shadowing effects.

Our results show a prominent spatial and angular variability in LAI values within the studied floodplain across the -36°, nadir and +36° VZAs (figure 4). When comparing LAI retrievals from the different angles, it appeared that the -36° VZA demonstrated largest variability and best retrieval performances. Particularly subtle LAI variations in case of low LAI were best detected in this viewing configuration (figure 4[top]). An explanation for this observation is that the -36° VZA approached the hotspot most closely, which implies the least influence of shadowing effects and therefore an enhanced richness of subtle variations in reflectance [23,58]. Such enhanced subtleties are assumed to be in a way related to an increased sensitivity towards structural variables [59,60], which makes the viewing angle closest to the hotspot of specific interest.

Slightly less accuracy and variability in LAI retrievals was observed in nadir VZA (figure 4[middle]). The lowest accuracy in LAI retrievals occurred at +36° VZA (figure 4[bottom]). In this direction most of the leaf surfaces are shaded, thereby suppressing variations in reflectance and thus sensitivity in assessing foliage density. Similar results but for a coarser resolution of 275 m were obtained with the usage of multi-angular broadband MISR data [61,62]. These studies underlined that

the surface anisotropy signatures varied with sun-target-sensor geometry as well as with seasonality due to changes in canopy composition and structure. Other studies [63,29] found increased sensitivities to vegetation structure and reduced understory effects in off-nadir viewing angles when compared to mono-directional nadir data. This evidence of increased sensitivity to vegetation structure supports the observation that the LAI retrievals from -36° VZA lead to superior results when compared to the conventional nadir VZA. However, as our results showed that the differences between -36° and nadir direction were rather small, which suggests that nadir observations are still a valid option.

4.2. Combined classification and radiative transfer modelling approach

Vegetation classification prior to model inversion proved to be a vital step for proper retrieval of biophysical parameters in heterogeneous or patchy landscapes. Effectively, one of the main drawbacks regarding the usage of RT models is the poor representation of the ensemble of vegetation structural variables and optical properties present in the field (e.g., [64-66]). RT models are typically parameterized for a specific land cover type, e.g., crops, forest, grassland, thereby restricting model inversion to this specific land cover type. However, in patchy or heterogeneous landscapes, such as river floodplains, it cannot be assumed that model parameterization for one vegetation type is valid for the whole landscape. In this respect, the proposed 1D/3D parameterization (along with distinct optical properties) per vegetation class ensures a more accurate representation of the landscape heterogeneity. From the generated LAI maps it can be observed that the three proposed classes of herbaceous, shrubs and forest proved to be valid within the floodplain of the Millingerwaard. Though, at the same time the fact that spurious high results appeared over agricultural (maize) areas in the larger region suggests that these areas fell not within the range of simulations that were parameterized according to the ‘herbaceous’ class. For improved LAI retrievals it would therefore be wise to consider these areas as a new class and parameterize the RT model accordingly.

A difficulty of vegetation class-based inversion is that it relies on a classified map of sufficient quality. Apart from the enriched information content for retrievals of vegetation density properties, pointable data can also enhance the classification process itself. For instance, here ROIs were identified with great precision because in certain PC-band combinations of the stacked layers of the three viewing angles the different classes had bright, distinctive colours. However, the potential of pointable data in the classification process has not yet been exploited to the fullest. In this study, classification was performed on the CHRIS nadir image only. Owing to the advantages of the multi-dimensionality of CHRIS, pointable observations may also be used as input into the classification method. For instance, [67] found that differences in classes were more evident in multi-angular band

compositions than in RGB true colour compositions. By using stacked layers of all multi-angular CHRIS observations as classification input instead of relying on solely the nadir image they improved the neural network classification results with 7%. Several other studies demonstrated the strength of multi-angular information in improving land cover classification [68,23]. The latter authors improved the classification accuracy with a combination of nadir and off-nadir data, because as such they were better able to catch the canopy characteristics. Further, in a study by [69] nadir classification accuracy was improved by using additional anisotropic information derived from reflectance ratios of different viewing angles from CHRIS data, enhanced with PCA. Given these examples, a next step would be to elaborate on a more standardized protocol using data from pointable imaging spectrometers so that classifications and vegetation density retrievals can be realized in a more operational way. Besides, a more precise land cover map as base map may also lead to more accurate LAI retrievals. Apart from the here applied Maximum Likelihood classification numerous alternative classifiers exist which may be more successful in heterogeneous areas, such as unsupervised classifiers, support vector machines, fuzzy classifiers, neural networks (see review [70]). Finally, when moving towards operational use, additional gain in accuracy can be achieved through *i*) synchronizing acquisition of field data with the satellite overpass , and *ii*) fine-tuning parameterization of vegetation classes for improved class-based model inversion.

4.3. Towards space-based river floodplain monitoring

Overall, this study profited from the availability of pointable hyperspectral CHRIS data and the advantages of the RT approach. With a physical model, the specific background and vegetation reflectances for each vegetation type were taken into account, which makes LAI retrievals more accurate [33]. Because no additional *in situ* calibration data sets were needed for this RT approach, the class-based model inversion was easily applied to the larger area of the Gelderse Poort, which demonstrated the suitability of this approach to map the floodplains of the whole river catchment.

While CHRIS data were successfully inverted into vegetation density variables, it should nonetheless not be forgotten that PROBA is not an operational spacecraft but was designed as a technology demonstrator. In fact PROBA was initially intended as a one year mission [28]. Currently no new multi-angular imaging spectrometer missions are planned to be launched. Conversely, there is a growing trend to design a new generation of imaging spectrometers with pointable capabilities. EnMAP is such an example with ± 30º off-nadir pointing capabilities that aims to deliver operational data products [71]. In addition, another upcoming superspectral spaceborne system, named Vegetation and Environmental New micro Spacecraft (VENµS), also has pointable capabilities within the range of

554 30º along and across track and will be launched in 2013 [72]. For both of these sensors, vegetation
555 monitoring of both crops and natural vegetation will be an important application domain. Our results
556 support that off-nadir images benefit to the retrieval of vegetation density parameters and may
557 therefore be of specific interest in view of these upcoming pointable sensors. Further study is required
558 to investigate the viewing angle effect on RT model inversion of vegetation properties, including the
559 consequences for changing temporal resolutions.

560 Regardless of progress with respect to refined LAI mapping, eventually one single hydraulic
561 roughness parameter is required by the river manager. It remains to be investigated whether LAI alone
562 would suffice for deriving hydraulic roughness estimates or if additional information is required.
563 Therefore, a next research step would be to explore LAI outcomes in conjunction with other relevant
564 structural variables that can be derived from space such as fractional vegetation cover and vegetation
565 height [13]. Straatsma and Baptist [12] used both spectral and altimetry airborne data sets to estimate
566 roughness input parameters such as vegetation height and vegetation density, and subsequently used
567 these data as input into a hydrodynamic model to compute hydraulic roughness values of a local river
568 floodplain. When having a vegetation class map of the larger area available, class-based inversion of
569 LAI can be easily upscaled to a whole river catchment area. Compared to the traditional ecotope
570 approach spaceborne optical data offer a standardized, spatially-explicit and repeatable methodology
571 that can cover complete river catchments with high spatial detail. Benefitting from the enriched
572 information present in the backscatter direction, it is beyond doubt that operational pointable sensors
573 (e.g. EnMAP, VENµS) will play an important role in monitoring programmes. Given this all, further
574 research efforts should lie in elaborating on the compatibility of hydrodynamic models with
575 spaceborne-derived input variables.
576
577
578 **5. Conclusions**
579
580 Pointable imaging spectrometers possess advanced capabilities to observe vegetation under a
581 preferred viewing angle. The use of pointable CHRIS images for mapping vegetation density of a river
582 floodplain in the Netherlands was investigated. The spatial distribution of leaf area index (LAI) was
583 estimated from CHRIS data using the ray tracing model FLIGHT. The CHRIS nadir image was first
584 classified into three distinct vegetation classes (‘herbaceous’, ‘shrubs’, ‘forest’) that formed the basis
585 for class-based model inversion. By configuring FLIGHT per vegetation class a more accurate
586 representation of the heterogeneous nature of a river floodplain can be achieved, e.g., herbaceous and
587 shrubs were simulated in 1D mode while forest was simulated in 3D mode. LAI values were

588 subsequently pixelwise and class-based derived through model inversion, and this for each view zenith
589 angle (VZA: -36°, nadir, +36°) separately. LAI retrievals matched best with validation data at -36°
590 backscatter direction, which is the viewing angle that was positioned near to the solar position, closely
591 followed by nadir VZA. Also most LAI variability was observed in these two viewing angles. This
592 suggests that in absence of pointable observations nadir-based observations would be perfectly
593 appropriate for vegetation density monitoring applications. The forward scatterer +36° VZA led to
594 considerably poorer retrievals and is not recommended to be used for quantifying vegetation density.
595 The here proposed methodology has been implemented in a software package ARTMO. With ARTMO
596 LAI maps over larger areas can be generated in a semi-automatic way, while at the same time the
597 heterogeneous nature of the landscape and the viewing configurations of the sensor have been properly
598 interpreted. This opens opportunities in view of upcoming operational sensors with pointing
599 capabilities such as EnMAP and VENμS.

600

601 **Acknowledgements**

602

603 J. Verrelst is supported by the FP7-PEOPLE-IEF-2009 grant (Grant Agreement 252237). This work
604 was partially supported by projects AYA2010-21432-C02-01 and CICYT-2010 funded by the Spanish
605 Ministry of Science and Innovation. J. P. Rivera is acknowledged for technical support.

606

607

608 **References**

609

610 1. Straatsma, M.; Schipper, A.; Van der Perk, M.; Van den Brink, C.; Leuven, R.; Middelkoop, H.
611 Impact of value-driven scenarios on the geomorphology and ecology of lower Rhine floodplains
612 under a changing climate. *Landscape Urban. Plann.* **2009**, *92*, 160-174.
613 2. Tol, R.S.J.; Van Der Grijp, N.; Olsthoorn, A.A.; Van der Werff, P.E. Adapting to Climate: A Case
614 Study on Riverine Flood Risks in the Netherlands. *Risk Anal.* **2003**, *23*, 575-583.
615 3. Bronstert, A. Floods and Climate Change: Interactions and Impacts. *Risk Anal.* **2003**. *23*, 545-557.
616 4. Pinter, N., Van der Ploeg, R.R., Schweigert, P., Hoefer, G. Flood magnification on the River
617 Rhine. *Hydrol. Process.* **2006**, *20*, 147-164.
618 5. Disse, M.; Engel, H. Flood events in the Rhine basin: Genesis, influences and mitigation. *Nat.*
619 *Hazards* **2001**, *23*, 271-290.
620 6. Middelkoop, H.; Daamen, K.; Gellens, D.; Grabs, W.; Kwadijk, J.C.J.; Lang, H.; Parmeti,
621 B.W.A.H.; Schädler, B.; Schulla, J.; Wilke, K. Impact of climate change on hydrological regimes
622 and water resources management in the Rhine basin. *Clim. Change* **2001**, *49*, 105-128.
623 7. Silva, W.; Klijn, F.; Dijkman, J. 2001. Room for the Rhine Branches in The Netherlands; What the
624 Research Has Taught Us. WLIDelft Hydraulics: Delft; RIZA: Arnhem. Delft Hydraulics report
625 R3294; 2001, RIZA report 03.

8. Van Stokkom, H.T.C.; Smits, A.J.M. Flood defense in the Netherlands: A new era, a new approach. *Flood Defence*, B. Wu, Z. Wang, G. Wang, G.G.H. Huang, H. Fang and Jhuang (eds), New York: Science Press, **2002**, 34-47
9. Kooistra, L.; Wamelink, G.W.W.; Schaepman-Strub, G.; Schaepman, M.E.; Dobben, H.F. van, Aduaka, U.; Batelaan, O. Assessing and predicting biodiversity in a floodplain ecosystem: Assimilation of net primary prodution derived from imaging spectrometer data into a dynamic vegetation model. *Remote Sens. Environ.* **2008**, *112*, 2118 - 2130.
10. Baptist, M.J.; Penning, W.E.; Duel, H.; Smits, A.J.M.; Geerling, G.W.; Van Der Lee, G.E.M.; Van Alphen, J.S.L. Assessment of the effects of cyclic floodplain rejuvenation on flood levels and biodiversity along the Rhine river. *River Res. and Appl.* **2004**, *20*, 285-297.
11. Geerling, G.W.; Kater, E.; Van den Brink, C.; Baptist, M.J.; Ragas, A.M.J.; Smits, A.J.M. Nature rehabilitation by floodplain excavation: The hydraulic effect of 16 years of sedimentation and vegetation succession along the Waal River, NL. *Geomorphology* **2008**, *99*, 317–328.
12. Straatsma, M.W.; Baptist, M.J. Floodplain roughness parameterization using airborne laser scanning and spectral remote sensing. *Remote Sens. Environ.* **2008**, *112*, 1062-1080.
13. Duel H.; Baptist M.J.; Penning W.E. Cyclic Floodplain Rejuvenation: A New Strategy Based on Floodplain Measures for Both Flood Risk Management and Enhancement of the Biodiversity of the River Rhine. NCR publication, Delft, **2001**, 14.
14. Van Velzen, E.H.; Jesse, P.; Cornelissen, P.; Coops, H. 2003. Stromingsweerstand vegetatie in uiterwaarden, deel 1 handboek. RIZA rapport, Arnhem: RIZA, **2003**, 028.
15. Jonckheere, I.; Fleck, S.; Nackaerts, K.; Muysa, B.; Coppin, P.; Weiss, M.; Baret, F. Review of methods for in situ leaf area index determination Part I. Theories, sensors and hemispherical photography. *Agric. For. Meteorol.* **2004**, *121*, 19-35.
16. Forzieri, G.; Guarnieri, L.; Vivoni, E.R.; Castelli, F.; Preti, F. Spectral-ALS data fusion for different roughness parameterizations of forested floodplains. *River Res. Appl.* **2011**, *27*, 826-840.
17. Baret, F.; and Guyot, G. Potentials and limits of vegetation indices for LAI and APAR assessment. *Remote Sens. Environ.* **1991**, *35*, 161-173.
18. Broge, N. H.; Leblanc, E. Comparing prediction power and stability of broadband and hyperspectral vegetation indices for estimation of green leaf area index and canopy chlorophyll density. *Remote Sens. Environ.* **2001**, *76*, 156-172.
19. Verrelst, J.; Schaepman, M.; Malenovsky, Z.; Clevers, J. Effects of woody elements on forest canopy chlorophyll content retrieval. *Remote Sens. Environ.* **2010**, *114*, 647-656.
20. Ross, J., The radiation regime and architecture of plant stands. Dr W. Junk Publishers, The Hague-Boston-London, **1981**.
21. Baret, F.; Weiss, M.; Troufleau, D.; Prevot, L.; Combal, B. Maximum information exploitation for canopy characterization by remote sensing. *Aspect Appl. Biol.* **2000**, *60*, 71-82.
22. Rautiainen, M.; Stenberg, P.; Nilson, T.; Kuusk, A. The effect of crown shape on the reflectance of coniferous stands. *Remote Sens. Environ.* **2004**, *89*, 41-52.
23. Sandmeier, S.; Deering, D.W. Structure Analysis and Classification of Boreal Forests Using Airborne Hyperspectral BRDF Data from ASAS. *Remote Sens. Environ.* **1999**, *69*, 281-295.
24. North, P.R.J. Three-dimensional Forest Light Interaction Model using a Monte Carlo method. *IEEE Trans. Geosci. Remote Sens.* **1996**, *34*, 946-956.
25. Diner, D. J.; Asner, G.P.; Davies, R.; Knyazikhin, Y.; Muller, J-P.; Nolin, A.W.; Pinty, B.; Schaaf, C.B.; Stroeve, J. New Directions in Earth Observing: Scientific Applications of Multiangle Remote Sensing. *Bull. Amer. Meteor. Soc.* **1999**, *80*, 2209-2228.

26. Chen, J. M.; Liu, J.; Leblanc, S.G.; Lacaze, R.; Roujean, J-L. Multi-angular optical remote sensing for assessing vegetation structure and carbon absorption. *Remote Sens. Environ.* **2003**, *84*, 516-525.
27. Diner, D. J.; Braswell, B.H.; Davies, R.; Gobron, N.; Hu, J.; Jin, Y.; Kahn, R.A.; Knyazikhin, Y.; Loeb, N.; Muller, J-P.; Nolin, A.W.; Pinty, B.; Schaaf, C.B.; Seiz, G.; Strove, J. The value of multiangle measurements for retrieving structurally and radiatively consistent properties of clouds, aerosols, and surfaces. *Remote Sens. Environ.* **2005**, *97*, 495-518.
28. Barnsley, M. J.; Settle, J.J.; Cutter, M.A.; Lobb, D.R.; Teston, F. The PROBA/CHRIS mission: A low-cost smallsat for hyperspectral multiangle observations of the earth surface and atmosphere. *IEEE Trans. Geosci. Remote Sens.* **2004**, *42*, 1512-1520.
29. Heiskanen, J. Tree cover and height estimation in the Fennoscandian tundra–taiga transition zone using multiangular MISR data. *Remote Sens. Environ.* **2006**, *103*, 97-114.
30. Pocewicz, A.; Vierling, L.A.; Lentile, L.B.; Smith, R. View angle effects on relationships between MISR vegetation indices and leaf area index in a recently burned ponderosa pine forest. *Remote Sens. Environ.* **2007**, *107*, 322-333.
31. Chopping, M.; Moisen, G.G.; Su, L.; Laliberte, A.; Rango, A.; Martonchik, J.V.; Peters, D.P.C. Large area mapping of southwestern forest crown cover, canopy height, and biomass using the NASA Multiangle Imaging Spectro-Radiometer. *Remote Sens. Environ.* **2008**, *112*, 2051-2063.
32. Sandmeier, S.; Müller, C.; Hosgood, B.; Andreoli, G. Physical mechanisms in hyperspectral BRDF data of grass and watercress. *Remote Sens. Environ.* **1998**, *66*, 222-233.
33. Richter, K.; Timmermans, W.J. Physically based retrieval of crop characteristics for improved water use estimates. *Hydrol. Earth Syst. Sc.* **2009**, *13*, 663-674.
34. Migdall, S.; Bach, H.; Bobert, J.; Wehrhan, M. Inversion of a canopy reflectance model using hyperspectral imagery for monitoring wheat growth and estimating yield. *Precis. Agr.* **2009**, *10*, 508-524.
35. Verrelst, J.; Schaepman, M.; Koetz, B.; Kneubühler, M. Angular sensitivity analysis of vegetation indices derived from CHRIS/PROBA data. *Remote Sens. Environ.* **2008**, *112*, 2341-2353.
36. Verrelst, J.; Geerling, G.W.; Sykora, K.V.; Clevers, J.G.P.W. Mapping of aggregated floodplain plant communities using image fusion of CASI and LiDAR data. *Int. J. Appl. Earth Obs. Geoinf.* **2009**, *11*, 83-94.
37. Ma, J.; Chan, J.C.-W.; Canters, F. Fully Automatic Subpixel Image Registration of Multiangle CHRIS/Proba Data. *IEEE Trans. Geosci. Remote Sens.* **2010**, *48*, 2829-2839.
38. Guanter, L.; Alonso, L.; Moreno, J. A method for the surface reflectance retrieval from PROBA/CHRIS data over land: Application to ESA SPARC campaigns. *IEEE Trans. Geosci. Remote Sens.* **2005**, *43*, 2908-2917.
39. Lotsch, A.; Tian, Y.; Friedl, M.A.; Myneni, R.B., Land cover mapping in support of LAI and FPAR retrievals from EOS-MODIS and MISR: Classification methods and sensitivities to errors. *Int. J. Remote Sens.* **2003**, *24*, 1997-2016.
40. Dorigo W.; Richter R.; Baret F.; Bamler R.; Wagner W. Enhanced Automated Canopy Characterization from Hyperspectral Data by a Novel Two Step Radiative Transfer Model Inversion Approach. *Remote Sens.* **2009**, *1*, 1139-1170.
41. Geerling, G.W.; Kater, E.; Van den Brink, C.; Baptist, M.J.; Ragas, A.M.J.; Smits, A.J.M. Nature rehabilitation by floodplain excavation: The hydraulic effect of 16 years of sedimentation and vegetation succession along the Waal River, NL. *Geomorphology* **2008**, *99*, 317–328.

42. Broadbent, E.N.; Zarin, D.J.; Asner, G. P.; Peña-Claros, M.; Cooper, A.; Littell, R. Recovery Of Forest Structure And Spectral Properties After Selective Logging In Lowland Bolivia. *Ecol. Appl.* **2006**, *16*, 1148-1163.
43. Gensuo, J.J.; Burke, I.C.; Goetz, A.F.H.; Kaufmann, M.R.; Kindel, B.C. Assessing spatial patterns of forest fuel using AVIRIS data. *Remote Sens. Environ.* **2006**, *102*, 318-327.
44. Guerschman, J.P.; Hill, M.J.; Renzullo, L.J.; Barrett, D.J.; Marks, A.S.; Botha, E. J. Estimating fractional cover of photosynthetic vegetation, non-photosynthetic vegetation and bare soil in the Australian tropical savanna region upscaling the EO-1 Hyperion and MODIS sensors. *Remote Sens. Environ.* **2009**, *113*, 928-945.
45. Kimes, D. S.; Nelson, R. F.; Manry, M. T.; Fung, A. K., Attributes of neural networks for extracting continuous vegetation variables from optical and radar measurements. *Int. J. Remote Sens.* **1998**, *19*, 2639-2662.
46. Schlerf, M.; Atzberger, C. Inversion of a forest reflectance model to estimate structural canopy variables from hyperspectral remote sensing data. *Remote Sens. Environ.* **2006**, *100*, 281-294.
47. Darvishzadeh, R.; Skidmore, A.; Schlerf, M.; Atzberger, C. Inversion of a radiative transfer model for estimating vegetation LAI and chlorophyll in a heterogeneous grassland. *Remote Sens. Environ.* **2008**, *112*, 2592-2604.
48. Kimes, D. S.; Knyazikhin, Y.; Privette, J. L.; Abuelgasim, A. A.; Gao, F. Inversion methods for physically-based models *Remote Sens. Rev.* **2000**, *18*, 381-439.
49. Combal, B.; Baret, F., and Weiss, M. Improving canopy variables estimation from remote sensing data by exploiting ancillary information. Case study on sugar beet canopies. *Agronomie* **2002**, *22*, 205-215.
50. Richter, K.; Atzberger, C.; Vuolo, F.; Weihs, P.; D'Urso, G. Experimental assessment of the Sentinel-2 band setting for RTM-based LAI retrieval of sugar beet and maize. *Can. J. Remote Sens.* **2009**, *35*, 230-247.
51. Vohland, M.; Mader, S.; Dorigo, W. Applying different inversion techniques to retrieve stand variables of summer barley with PROSPECT + SAIL. *Int. J. Appl. Earth Obs. Geoinf.* **2010**, *12*, 71-80.
52. Schaepman, M.E.; Wamelink, G.W.W.; Dobben, H.F. van, Gloor, M.; Schaepman-Strub, G.; Kooistra, L.; Clevers, J.G.P.W.; Schmidt, A.M.; Berendse, F. River floodplain vegetation scenario development using imaging spectroscopy derived products as input variables in a dynamic vegetation model. *Photogramm. Eng. Remote Sensing* **2007**, *73*, 1179-1188.
53. Justice, C.; Belward, A.; Morisette, J.; Lewis, P.; Privette, J.; Baret, F. Developments in the 'validation' of satellite sensor products for the study of the land surface. *Int. J. Remote Sens.* **2000**, *21*, 3383-3390.
54. Mengesha, T.; Schaepman, M.E.; De Bruin, S.; Zurita-Milla, R.; Kooistra, L. Ground validation of biophysical products using imaging spectroscopy in softwood forests, Proceedings of the VALERI Workshop, Baret, F. and Weiss, M. (eds.), INRA, Avignon, France, unpaginated CD-ROM, **2005**.
55. Clevers, J.G.P.W.; Kooistra, L. AHS2005: The 2005 airborne imaging spectroscopy campaign in the Millingerwaard, the Netherlands. **2008**, *CGI Report* 2008-001, ISSN 1568-1874. Wageningen University, Centre for Geo-Information
56. De Santis, A.; Chuvieco, E. Burn severity estimation from remotely sensed data: Performance of simulation versus empirical models. *Remote Sens. Environ.* **2007**, *108*, 422-435.
57. Verrelst, J.; Rivera J.P.; Alonso, L.; Moreno, J. ARTMO: an Automated Radiative Transfer Models Operator toolbox for automated retrieval of biophysical parameters through model

760 inversion In *Proceedings of 7th EARSeL Workshop on Imaging Spectrometry*, Edinburgh, UK, 11-13
761 April **2011**.
762 *58.* Dorigo, W.A. Improving the robustness of cotton status characterisation by radiative transfer
763 model inversion of multi-angular CHRIS/PROBA data *IEEE J. Sel. Top. Appl. Earth Obs. Remote*
764 *Sens.* **2012**, *5*, 18-29.
765 59. Weiss, M.; Baret, F.; Myneni, R.B.; Pragnère, A.; Knyazikhin, Y. Investigation of a model
766 inversion technique to estimate canopy biophysical variables from spectral and directional
767 reflectance data. *Agronomie* **2000**, *20*, 3-22.
768 60. Simic, A.; Chen, J.M. Refining a hyperspectral and multiangle measurement concept for
769 vegetation structure assessment. *Can. J. Remote Sens.* **2008**, *34*, 174-191.
770 61. Liesenberg, V.; Galvão, L.S.; Ponzoni, F.J. Variations in reflectance with seasonality and viewing
771 geometry: Implications for classification of Brazilian savanna physiognomies with MISR/Terra
772 data. *Remote Sens. Environ.* **2007**, *107*, 276-286.
773 62. Xavier, A.S.; Galvão, L.S. View angle effects on the discrimination of selected Amazonian land
774 cover types from a principal-component analysis of MISR spectra. *Int. J. Remote Sens.* **2005**, *26*,
775 3797-3811.
776 63. Rautiainen, M.; Lang, M.; Mõttus, M.; Kuusk, A.; Nilson, T.; Kuusk, J.; Lükk, T. Multi-angular
777 reflectance properties of a hemiboreal forest: An analysis using CHRIS PROBA data. *Remote*
778 *Sens. Environ.* **2008**, *112*, 2627-2642.
779 64. Gond, V.; De Pury, D.G.G.; Veroustraete, F.; Ceulemans, R. Seasonal variations in leaf area
780 index, leaf chlorophyll, and water content; Scaling-up to estimate fAPAR and carbon balance in a
781 multilayer, multispecies temperate forest. *Tree Phys.* **1999**, *19*, 673-679.
782 65. Soudani, K.; François, C.; le Maire, G.; Le Dantec, V.; Dufrêne, E. Comparative analysis of
783 IKONOS, SPOT, and ETM+ data for leaf area index estimation in temperate coniferous and
784 deciduous forest stands. *Remote Sens. Environ.* **2006**, *102*, 161-175.
785 66. Zhang, Q.; Xiao, X.; Braswell, B.; Linder, E.; Baret, F.; Moore Iii, B. Estimating light absorption
786 by chlorophyll, leaf and canopy in a deciduous broadleaf forest using MODIS data and a radiative
787 transfer model. *Remote Sens. Environ.*, **2005**, *99*, 357-371.
788 67. Duca, R.; Del Frate, F. Hyperspectral and multiangle CHRIS-PROBA images for the generation of
789 land cover maps. *IEEE Trans. Geosci. Remote Sens.* **2008**, *46*, 2857-2866.
790 68. Braswell, B.H.; Hagena, S.C.; Frolkinga, S.E.; Salas, W.A. A multivariable approach for mapping
791 sub-pixel land cover distributions using MISR and MODIS: Application in the Brazilian Amazon
792 region. *Remote Sens. Environ.* **2003**, *87*, 243-265.
793 69. Galvão, L.S.; Ponzoni, F.J.; Liesenberg, V.; Dos Santos, J.R. Possibilities of discriminating
794 tropical secondary succession in Amazônia using hyperspectral and multiangular CHRIS/PROBA
795 data. *Int. J. Appl. Earth Obs. Geoinf.* **2009**, *11*, 8-14.
796 70. Lu, D.; Weng, Q. A survey of image classification methods and techniques for improving
797 classification performance. *Int. J. Remote Sens.* **2007**, *28*, 823-870.
798
799 71. Stuffler, T.; Kaufmann, C.; Hofer, S.; Förster, K.P.; Schreier, G.; Mueller, A.; Eckardt, A.; Bach,
800 H.; Penné, B.; Benz, U.; Haydn, R. The EnMAP hyperspectral imager-An advanced optical
801 payload for future applications in Earth observation programmes. *Acta Astronaut.* **2007**, *61*, 115-
802 120.
803 72. Hermann, I.; Pimstein, A.; Karnieli, A.; Cohen, Y.; Alchanatis, V.; Bonfil, D.J. LAI assessment of
804 wheat and potato by VENμS and Sentinel-2 bands. *Remote Sens. Environ.* **2011**, *1*, 2141-2151.